Measurement of short-range correlations in nuclei at $x > 1$ with the quasi-elastic $(\vec{\mathrm{e}}, \mathrm{e}')$ process

Z. Ye,[1,2] J. Arrington,[3] D. Day,[1] D. W. Higinbotham,[4] P. Solvignon,[4,5] P. Aguilera,[6] Z. Ahmed,[7] H. Albataineh,[8] K. Allada,[9] B. Anderson,[10] D. Anez,[11] K. Aniol,[12] J. Annand,[13] W. Armstrong,[14] T. Averett,[15] T. Badman,[5] H. Baghdasaryan,[1] X. Bai,[16] A. Beck,[17] S. Beck,[17] V. Bellini,[18] F. Benmokhtar,[19] W. Bertozzi,[20] J. Bittner,[21] W. Boeglin,[22] A. Camsonne,[4] C. Chen,[23] J.-P. Chen,[4] K. Chirapatpimol,[1] E. Cisbani,[24] M. M. Dalton,[1] A. Daniel,[25] C. W. de Jager,[4,1] R. De Leo,[26] W. Deconinck,[20] M. Defurne,[27] D. Flay,[14] N. Fomin,[28] M. Friend,[19] S. Frullani,[24] E. Fuchey,[14] F. Garibaldi,[24] D. Gaskell,[4] S. Gilad,[20] R. Gilman,[29,4] O. Glamazdin,[30] C. Gu,[1] P. Gueye,[23] D. Hamilton,[13] C. Hanretty,[31] J.-O. Hansen,[4] M. Hashemi Shabestari,[1] O. Hen,[32] T. Holmstrom,[21] M. Huang,[2] S. Iqbal,[12] G. Jin,[1] N. Kalantarians,[33] H. Kang,[34] A. Kelleher,[20] M. Khandaker,[32] I. Korover,[32] J. LeRose,[4] J. Leckey,[35] R. Lindgren,[1] E. Long,[5] J. Mammei,[36] D. J. Margaziotis,[12] P. Markowitz,[22] A. Marti Jimenez-Arguello,[37] D. Meekins,[4] Z. Meziani,[14] R. Michaels,[4] M. Mihovilovic,[38] P. Monaghan,[20] N. Muangma,[20,23] C. Munoz Camacho,[37] B. Norum,[1] Nuruzzaman,[39] K. Pan,[20] S. Phillips,[5] E. Piasetzky,[32] I. Pomerantz,[32,40] M. Posik,[14] V. Punjabi,[41] X. Qian,[2] Y. Qiang,[2] X. Qiu,[42] P. E. Reimer,[3] A. Rakhman,[7] S. Riordan,[1,43] G. Ron,[44] O. Rondon-Aramayo,[4] A. Saha,[4,*] E. Schulte,[29] L. Selvy,[10] A. Shahinyan,[45] R. Shneor,[32] S. Sirca,[46] J. Sjoegren,[13] K. Slifer,[5] N. Sparveris,[14] R. Subedi,[1] V. Sulkosky,[20,21] W. Tireman,[47] D. Wang,[1] J. W. Watson,[10] L. B. Weinstein,[8] B. Wojtsekhowski,[4] S. A. Wood,[4] W. Yan,[48] I. Yaron,[32] X. Zhan,[20] J. Zhang,[4] Y. Zhang,[29] B. Zhao,[15] Z. Zhao,[1] X. Zheng,[1] P. Zhu,[48] and R. Zielinski[5]

(The Jefferson Lab Hall A Collaboration)

[1]*University of Virginia, Charlottesville, VA 22904*
[2]*Duke University, Durham, NC 27708*
[3]*Physics Division, Argonne National Laboratory, Argonne, IL 60439*
[4]*Thomas Jefferson National Accelerator Facility, Newport News, VA 23606*
[5]*University of New Hampshire, Durham, NH 03824*
[6]*Institut de Physique Nucléaire (UMR 8608), CNRS/IN2P3 - Université Paris-Sud, F-91406 Orsay Cedex, France*
[7]*Syracuse University, Syracuse, NY 13244*
[8]*Old Dominion University, Norfolk, VA 23529*
[9]*University of Kentucky, Lexington, KY 40506*
[10]*Kent State University, Kent, OH 44242*
[11]*Saint Mary's University, Halifax, Nova Scotia, Canada*
[12]*California State University, Los Angeles, Los Angeles, CA 90032*
[13]*University of Glasgow, Glasgow G12 8QQ, Scotland, United Kingdom*
[14]*Temple University, Philadelphia, PA 19122*
[15]*College of William and Mary, Williamsburg, VA 23187*
[16]*China Institute of Atomic Energy, Beijing, China*
[17]*Nuclear Research Center Negev, Beer-Sheva, Israel*
[18]*Universita di Catania, Catania, Italy*
[19]*Carnegie Mellon University, Pittsburgh, PA 15213*
[20]*Massachusetts Institute of Technology, Cambridge, MA 02139*
[21]*Longwood University, Farmville, VA 23909*
[22]*Florida International University, Miami, FL 33199*
[23]*Hampton University, Hampton, VA 23668*
[24]*INFN, Sezione Sanità and Istituto Superiore di Sanità, 00161 Rome, Italy*
[25]*Ohio University, Athens, OH 45701*
[26]*INFN, Sezione di Bari and University of Bari, I-70126 Bari, Italy*
[27]*CEA Saclay, F-91191 Gif-sur-Yvette, France*
[28]*University of Tennessee, Knoxville, TN 37996*
[29]*Rutgers, The State University of New Jersey, Piscataway, NJ 08855*
[30]*Kharkov Institute of Physics and Technology, Kharkov 61108, Ukraine*
[31]*Florida State University, Tallahassee, FL 32306*
[32]*Tel Aviv University, Tel Aviv 69978, Israel*
[33]*University of Texas, Houston, TX 77030*
[34]*Seoul National University, Seoul, Korea*
[35]*Indiana University, Bloomington, IN 47405*
[36]*Virginia Polytechnic Inst. and State Univ., Blacksburg, VA 24061*
[37]*Université Blaise Pascal/IN2P3, F-63177 Aubière, France*
[38]*Jozef Stefan Institute, Ljubljana, Slovenia*
[39]*Mississippi State University, Mississippi State, MS 39762*

[40]The University of Texas at Austin, Austin, Texas 78712
[41]Norfolk State University, Norfolk, VA 23504
[42]Lanzhou University, Lanzhou, China
[43]University of Massachusetts, Amherst, MA 01006
[44]Racah Institute of Physics, Hebrew University of Jerusalem, Jerusalem, Israel
[45]Yerevan Physics Institute, Yerevan 375036, Armenia
[46]University of Ljubljana, Ljubljana, Slovenia
[47]Northern Michigan University, Marquette, MI 49855
[48]University of Science and Technology, Hefei, China
(Dated: March 30, 2015)

We present new results of short-range correlations (SRC) with the measurement of electron scattering off high-momentum nucleons in a wide range of nuclei performed in Hall A at Jefferson Lab. The inclusive cross section ratio of ^{4}He to ^{3}He conforms the well-known two-nucleon short-range correction (2N-SRC) plateau in $1 < x < 2$ but yields a different pattern when extending to the $x > 2$ regime where previous measurements claimed an onset of the three-nucleon short-range correlation (3N-SRC) under a similar kinematic region. The ^{12}C to ^{3}He and ^{12}C to ^{4}He cross section ratios also show no indication of 3N-SRC plateau. We also present the first measurement of the ^{48}Ca to ^{40}Ca cross section ratio and the result indicates the universality of two-nucleon corrections for high-momentum nucleons in the isotopes.

PACS numbers: TBD

Understanding the complex structure of nuclei remains as one of the major tasks in nuclear physics. Short-range correlations (SRC) play an important rule to the formation of the nuclear structure but yet be well studied. The mighty repulsive core of the nucleon-nucleon (NN) interactions at short distance boosts the correlated nucleons' well above the Fermi momentum, while the nucleus remains in its ground state due to the momentum conservation. Without involving these high momentum components, the mean field calculation using the distorted wave impulse approximation [1] underestimated the nuclear strength which had been observed by many proton knock-out experiments [2–4].

Previous data revealed an asymptotic form of the momentum distributions for struck nucleons orginally from light nuclei and heavy nuclei [5]. It showed at moderate high momentum from 300 MeV to 600 MeV, the distributions of heavy nuclei scale to the one of the deuteron. It could be easily understood if the 2N-SRC pair shares the similar features among different nuclei. One also suggested that the momentum distributions should scale to the one of ^{3}H or ^{3}He for the much higher momentum tail where 3N-SRC configuration dominates [6].

Instead of direclty investigating the momentum distribution of the nucleus which is not an experimental observable, one can study the SRC via inclusive electrons quasielastic (QE) scattering off nuclei [7]. During the scattering, the electron gives up its energy via emitting a virtual photon with the four momentum transfer $Q^2 = |\vec{q}|^2 - \nu^2$, where $\vec{q}$ and ν are the momentum and energy of the virtual photon. The interaction between the virtual photon and the nucleon provides an unique probe to study the nucleon's intial state, e.g., the momentum distribution which is correlated to the scaling function [7–11]:

$$F(y) = 2\pi \int_{|y|}^{\infty} n(p_0) \cdot p_0 dp_0, \tag{1}$$

where $n(p_0)$ is the momentum distribution of the nucleon with the initial momentum p_0. y is the solution of $M_A + \nu = \sqrt{M^2 + |\vec{q}|^2 + y^2 + 2y|\vec{q}|} + \sqrt{M_{A-1}^2 + y^2}$ where M, M_A and M_A are the masses of the nucleon, target nucleus A and the (A-1) recoil system, respectively. $F(y)$ can be directly extracted from the experimental QE inclusive cross section:

$$F(y) = \frac{d^3\sigma_{EX}}{dE'd\Omega} \frac{1}{Z\sigma_p + N\sigma_n} \frac{q}{\sqrt{M^2 + (y+q)^2}}, \tag{2}$$

where σ_p and σ_n are the electron-proton and electron-neutron cross section, respectively.

Compared with the electrons elastic scattering process which is well peaked at $x = Q^2/2Mv = 1$ (M is the proton mass), the QE process yields a much broader peaks at $x = 1$ due to the Fermi motion of the nucleon inside the nucleus. By measuring the inclusive QE cross section at $x > 1$ with $Q^2 > 1\ GeV^2$, one can carefully map out the SRC in different nuclei by taking the cross section ratio of the heavy nucleus, A, to the light nuclei, e.g. deuteron or ^{3}He:

$$a_D(A) = \frac{2}{A} \frac{\sigma_A(x, Q^2)}{\sigma_D(x, Q^2)}, a_{^3He}(A) = \frac{3}{A} \frac{\sigma_A(x, Q^2)}{\sigma_{^3He}(x, Q^2)}, \tag{3}$$

where $2/A$ or $2/A$ accounts for the possibilities of forming SRC configurations in different nuclei similar to deuteron or ^{3}He.

The first study of the SRC via the inclusive scattering was revealed by the SLAC data [12] which revealed a 2N-SRC plateau on the $a_D(A)$ started to raise at $x \sim 1.5$.

A recent measurement from the CLAS data in Hall B at JLab [13] reported a more clear 2N-SRC plateau on the $a_{^3He}(A)$ distribution. The latest measurement was performed by the E02-019 experiment from Hall C at JLab with better precision and a wider range of nuclei, and both $a_D(A)$ and $a_{^3He}(A)$ show clear 2N-SRC plateau [14]. The CLAS data claimed a second plateau at $x > 2$ in the $\sigma_{^4He}/\sigma_{^3He}$ ratio. However, the E02-19 result presented a different approach in this region despite the large error bars due to the lack of statistics. The discrepancy between these two measurements can not be explained at this stage. One of the facts is that both experiments ran at very different Q^2 while the kinematic requirement of performing clean measurements of 3N-SRC is not well understood yet.

The new JLab experiment, E08-014, was carried out in Hall A in 2011 [15] and focused on the measurements of inclusive cross sections at large x with high precision. An high intensity electron beam with a constant energy of 3.356 GeV was employed to the hall and struck on fixed targets, and the scattered electrons were simultaneously detected by two identical High-Resolution Spectrometers (HRSs) [16]. Three 20 cm long cryogenic targets, the ^{2}D liquid, the ^{3}He gas and the ^{4}He gas, were used, in addition to thin foils of ^{12}C, ^{40}Ca and ^{48}Ca. Each HRS consists of a pair of vertical drift chambers (VDCs) for particle tracking, two scintillator planes for triggering and timing measurements, and a gas Čerenkov counter and two layers of lead-glass calorimeters for particle identification. The spectrometers were positioned at $\theta_0 = 21°$, $23°$, $25°$, and $28°$ with total of 9 different central momentum settings, which cover the Q^2 range from 1.1 (GeV/c)^2 upto 2.5 (GeV/c)^2. The detailed description of the experiment and the data analysis can be found in Ref. [17].

The HRS detectors had very high electron detection capability and the event rate of this experiment was low since the cross section drops exponentially away from the QE peak. Events with only one-track from the VDCs' tracking reconstruction were kept for analysis, while the zero-track and multi-track events were less than 1%. The efficiencies of the detectors were carefully evaluated and turned out to be close to 100% even with the highest event rates. No further correction was applied. The electrons were identified by applying combination cuts on the calibrated signals from both the Čerenkov detector and the calorimeters. The cuts were able to keep above 99% electrons while the pion to electron ratio was estimated to be better than 10^{-4} level thanks to the low pion production rate under these kinematic regions. The overall dead-time of our data acquisition system (DAQ) was evaluated and corrected for each run.

The scattered electron's outgoing momentum, in-plan and out-of-plan angles and its vertex position on the target can be reconstructed with the optics matrices of the HRSs using the tracking information from the VDCs as inputs. The optics matrices have been well calibrated by many previous Hall A experiments and it were also optimized with the new calibration data taken during this experiment.s The uncertainty from the optics reconstruction is believed to be better than 99% [16]. To reduce the edge effects due to the spectrometers' geometries, only the central acceptance regions were chose by cutting on these reconstructed quantities. A Monte Carlo (MC) simulation of the HRSs [17] was employed to evaluate and correct for the residual acceptance effect.

For the cryogenic targets, we removed the contaminated events from electrons scattering off the end-cups of the target cells by applying a cut on the reconstructed vertex position of the scattered electron on the target. A dummy target of two thin aluminum foils with 20 cm apart was used to evaluate the level of residual contamination after the cut. With the precise optics reconstruction, a cut of $\pm 7\ cm$ at the center part of the target is able to remove $> 99.9\%$ of the events from target end-cups.

One of the largest sources of systematic uncertainty come from the non-uniform target densities of ^{2}D, ^{3}He and ^{4}He due to the not well distributed coolant flow and the high beam current from 40 muA up to 120 muA. We took the boiling study data on these target with varying beam currents, and extrapolated the density profiles when the beam was off and normalized the distribution to the values obtained during the target installation. For safety, we assigned 5% uncertainty of the target density for each cryogenic target.

(FIX-HERE: Discuss more about the systematic uncertainties from different sources and make a table).

The cross sections were extracted by binning the data in x. A yield ratio method was developed to apply all necessary corrections only on the MC data until the MC yield converges to the experimental yield in the same x bin. The experimental yield for the ith x bin is defined as:

$$Y^i_{EX} = \frac{N^i_{EX}}{N_e}, \tag{4}$$

where N^i_{EX} is the number of scattered electrons within the bin after all event selections and acceptance cuts, and N_e is the total number of incoming electrons hit on the target. The MC yield can be written as:

$$Y^i_{MC} = \epsilon_{eff} \cdot \eta_{tg} \cdot \frac{\Delta E'_{MC} \Delta\Omega_{MC}}{N^{gen}_{MC}} \cdot \sum_{j \in i} \sigma^{rad}_{model}(E_j, E'_j, \theta_j). \tag{5}$$

where ϵ_{eff} is the product of efficiencies from varied sources. η_{tg} denotes the areal density of the scattering centers calculated from the target thickness, $\eta_{tg} = \rho \cdot l \cdot N_A/A$ where N_A is the Avogadro's number. The target density has been corrected with the boiling effect. $\Delta E'_{MC}$ and $\Delta\Omega_{MC}$ are the momentum and solid angle overages of the HRS in the simulation which were chose to be slighly larger than the actuall ranges, and N^{gen}_{MC}

is the total number of generated MC events within the ranges. The terms in $\sum_{j\in i}$ represent that within the ith x-bin, the jth electron is first weighed by the radiated cross section calculated with the incoming beam energy E_j, outgoing momentum E'_j and angle θ_j and then summurized. A cross section model was developed based on the $F(y)$ scaling and the peaking-approximation method was used to calculate the radiation effect [17].

The experimental cross section for the ith bin is then given by:

$$\sigma_{EX}(E,E'_i,\theta_0) = \frac{Y^i_{EX}}{Y^i_{MC}} \cdot \sigma_{model}(E,E'_i,\theta_0), \quad (6)$$

where E is the beam energy fixed at 3.356 GeV, θ_0 is the central scattering angle, E'_i, the scattered energy, is calculated based on x_i, and $\sigma_{model}(E,E'_i,\theta_0)$ is the cross section of the bin calculated from the model with the radiation effect corrected. In this method, the bin-centering correction was automatically applied for choosing the center of the x-bin. The cross sections of different targets were extracted with exactly the same bins and the same acceptance cuts. Their statistical and systematic errors were individually calculated before taking the cross section ratio.

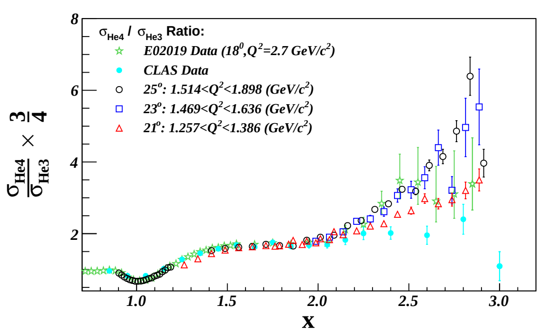

FIG. 1. Cross section ratio of ^4He to ^3He with this experiment at three Q^2 settings and also the results from E02-019 and CLAS. Statistical errors and systematic errors from instruments are included.

Fig. 1 gives the cross section ratio of ^{4}He to ^{3}He as a function of x. In the 2N-SRC region, the new data reveals a plateau which agrees nicely with the CLAS and E02-019 results. However, at $x > 2$, our result shows no 3N-SRC plateau which was claimed by the CLAS data, but instead, raises up quickly when x approaches 3 which tends to agree more with the E02-019 data despite its large errors. While E02-019 ran at higher Q^2, the situation becomes interesting that our data and the CLAS data were taken with the similar Q^2 range but yield different approaches, and it is ergent to be investigated further. A recent publication suggested that the 3N-SRC plateau showed in the CLAS data could be just a result of inappropriate binning and bin-centering correction [18].

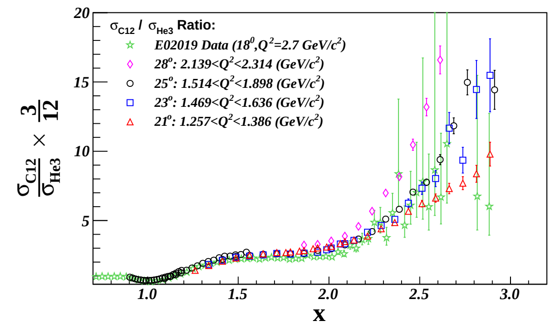

FIG. 2. Cross section ratio of ^{12}C to ^3He with this experiment at three Q^2 settings and also the results from E02-019. Statistical errors and systematic errors from instruments are included.

We also present the new results of the ^{12}C to ^3He ratio and the ^{12}C to ^4He ratio, as shown in Fig. 2 and Fig. 4, respectively. The E02-19 result of the ^{12}C to ^3He ratio is also included for comparing. The 2N-SRC plateaus are shown in both plots where there are no indication of the 3N-SRC plateau at large x.

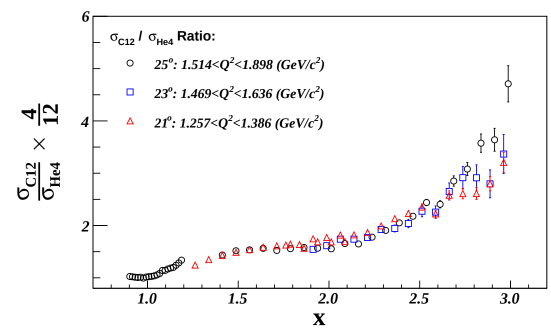

FIG. 3. Cross section ratio of ^{12}C to ^4He with this experiment at three Q^2 settings. Statistical errors and systematic errors from instruments are included.

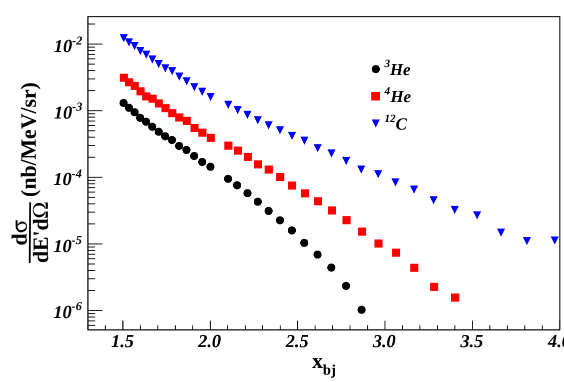

FIG. 4. Cross sections of ^3He, ^4He and ^{12}C at the 25° setting. Statistical errors and systematic errors from instruments are included.

(Add discussion here)

(Add statements here)

(Add conclusion here)

(Add acknowledgments here)

---

* deceased

[1] J. D. Forest, Nucl. Phys. **A392**, 232 (1983).

[2] G. V. D. Steenhoven *et al.*, Nuclear Physics A **480**, 547 (1988).

[3] L. Lapiks, Nuclear Physics A **553**, 297 (1993).

[4] J. Kelly, Adv. Nucl. Phys. **23**, 75 (1996).

[5] C. Ciofi degli Atti and S. Simula, Phys. Rev. C **53**, 1689 (1996).

[6] J. Arrington, D. Higinbotham, G. Rosner, and M. Sargsian, Progress in Particle and Nuclear Physics **67**, 898 (2012).

[7] O. Benhar, D. Day, and I. Sick, Rev. Mod. Phys. **80**, 189 (2008).

[8] G. B. West, Physics Reports **18**, 263 (1975).

[9] D. B. Day, J. S. McCarthy, T. W. Donnelly, and I. Sick, Annual Review of Nuclear and Particle Science **40**, 357 (1990).

[10] C. Ciofi degli Atti, S. Liuti, and S. Simula, Phys. Rev. C **41**, R2474 (1990).

[11] S. Boffi, C. Giusti, and F. Pacati, Physics Reports **226**, 1 (1993).

[12] L. L. Frankfurt, M. I. Strikman, D. B. Day, and M. Sargsyan, Phys. Rev. C **48**, 2451 (1993).

[13] CLAS Collaboration, K. S. Egiyan *et al.*, Phys. Rev. Lett. **96**, 082501 (2006).

[14] N. Fomin *et al.*, Phys. Rev. Lett. **105**, 212502 (2010).

[15] J. Arrington, D. Day, D. Higinbotham, and P. Solvignon, Three-nucleon short range correlations studies in inclusive scattering for $0.8 < Q^2 < 2.8(GeV/c)^2$, `http://hallaweb.jlab.org/experiment/E08-014/`, 2011.

[16] J. Alcorn *et al.*, Nucl. Instrum. Meth. **A522**, 294 (2004).

[17] Z. Ye, Ph.D Thesis, University of Virginia, 2013, arXiv:1408.5861.

[18] D. Higinbotham and O. Hen, Tbd, 2014.